Chapter 4

Prospective study of ITER-FEAT

4.1 Introduction

The present time is crucial for the next step in magnetic fusion. On the one hand, the world programme is scientifically and technically ready to take this next step, which is essential in order to continue the progress in fusion development, and at the moment several devices have been proposed. On the other hand, up to now, no decisions have been taken for carrying them out. The most important project is the international collaborative ITER, with a nominal energy plasma gain of $Q = 10$.

The aim of this Chapter is to evaluate and analyse the performance and sensitivity of such a device, by solving self-consistently the power balance equation (Eq. (2.1)) in a determinate mode of operation, taking into account both the degradation of the energy confinement time with the non-radiative total power and the imposed value of the ratio of the apparent helium particles confinement time to the energy confinement time $\tau^*_{\mathrm{He}}/\tau_E$. The following questions are principally treated:

- performance prediction in inductive mode of operation and analysis of operating margins;
- sensitivity of $\tau^*_{\mathrm{He}}/\tau_E$ to the plasma performance;
- operating point using a softly mixed scaling for the energy confinement time;
- performance prediction in the non-inductive mode of operation (continuous);
- role of the plasma density and confinement enhancement in non-inductive operation.

4.2 The ITER project

In recent years, the various fusion energy programmes throughout the world have benefited from a remarkable degree of openness and global cooperation which has brought with it dramatic progress in scientific understanding and performance achievement. The leading fusion experiments such as JET, JT-60 and TFTR, have reached their objectives and continue (except TFTR) exploring the fusion domain around the threshold of break-even conditions, while devices like Tore Supra are devoted to long time pulses, near the steady-state. Other smaller supporting experiments and theoretical developments are together broadening scientific understanding and establishing competence in fusion technologies.

The next step for all the world's leading fusion programmes is to progress in the study of burning plasma physics. Within the strategy of reaching an electricity-producing reactor with a minimum of steps, thus in a minimum time frame and global cost, the next logical step leads to the International Thermonuclear Experimental Reactor (ITER) project. The aim of such a project is to demonstrate the scientific and technological feasibility of fusion as a practical energy source.

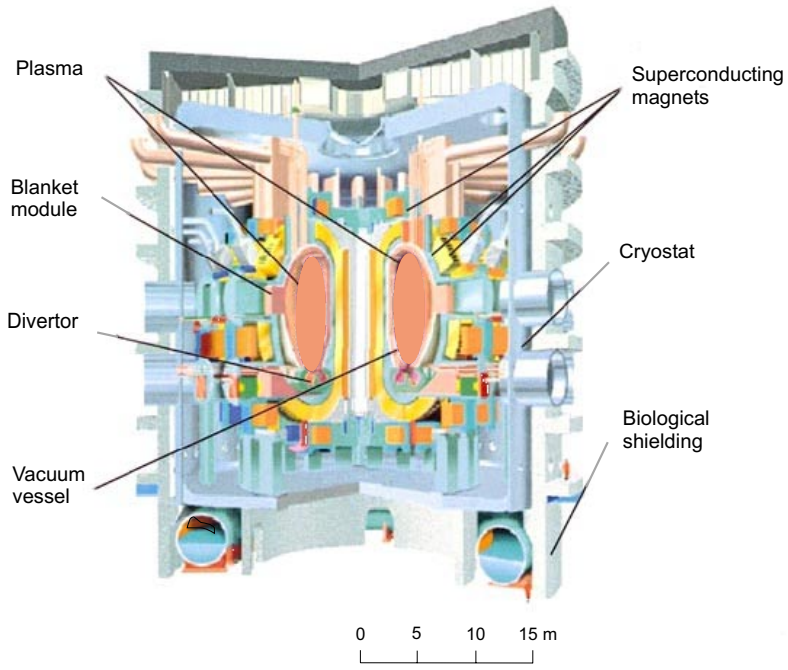

Figure 4.1: Schematic diagram of ITER-FEAT. Source: Naka (Japan) Joint Work Site of ITER.

The international collaboration on ITER offers significant savings through shar-

ing of costs, and more importantly, the opportunity to pool the experience and expertise gained over recent decades and to draw from the scientific and technological expertise of all the world's leading fusion experiments and programmes.

4.2.1 From ITER-FDR to ITER-FEAT(historical review)

At the Geneva Summit Meeting in November 1985, a proposal was made by the Soviet Union to build a next generation tokamak experiment on a collaborative basis involving the world's four major fusion programmes. In October 1986, the United States, in consultation with Japan and the European Community, responded with a proposal on how to implement such an activity. The ensuing discussions between diplomatic and technical representatives of the four prospective participants resulted in the establishment of a collaboration under the auspices of the International Atomic Energy Agency (IAEA).

Representatives of the four programmes developed a detailed proposal for co-operation on the Conceptual Design Activities (CDA) for ITER. In technical terms, the collaboration orientated the fusion research efforts of the various Parties towards a common goal. In addition, the process of the CDA and the successful addressing of organisational and human issues gave the Parties confidence that the project could move on to its next stage of engineering design activities as an international project under the terms of an inter-governmental collaborative agreement. In July 1992 the four Parties signed an Agreement, which established the Engineering Design Activities (EDA). Canada and Kazakhstan are also involved in the Project by association with Euratom and Russia respectively. The EDA was defined to produce a detailed, complete and fully integrated engineering design of ITER and all technical data necessary for future decisions on the construction of ITER. Six years of international collaborative work within the framework of the ITER EDA Agreement culminated in the approval by the ITER Council in June 1998 of the ITER Final Design Report, Cost Review and Safety Analysis (FDR) [FDR97]. The FDR provided the first comprehensive design of a fusion reactor based on well established physics and technology. Its design fulfilled the overall programmatic objective of ITER, i.e. to demonstrate the scientific and technological feasibility of fusion energy for peaceful purposes, and complied with the detailed technical objectives and technical approaches adopted by the ITER Parties at the start of the EDA.

At the time of the FDRs acceptance, the ITER Parties, recognising the possibility that they might be unable, for financial reasons, to proceed with the construction of the then foreseen device, deemed it prudent to make an available option for ITER, the cost of which would be cut by half by reducing the detailed technical objectives and possibly decreasing the technical margins while maintaining the overall programmatic objective of ITER.

The work was to follow the adopted technical guidelines and make the most cost-

effective use of existing design solutions and their associated R&D. The EDA was subsequently extended to July 2001 to cover this work, in spite of the US decision to leave the project by the end of its 1999 fiscal year. A device, which would achieve energy gain of at least $Q = 10$ and explore steady-state operation, at a direct capital cost of approximately 50% of the 1998 ITER design, would still satisfy the ITER overall programmatic objective. At the end of 1999, the key features of a device, referred to as ITER-FEAT, were provided for the ITER Parties in an Outline Design Report [ODR99].

4.3 Geometry, magnetic field, safety factor

The following nominal geometrical parameters of ITER-FEAT [ODR99] are assumed:

$$R = 6.20 \text{ m}, \quad a = 2.00 \text{ m}, \quad \kappa_{95} = 1.70, \quad \delta_{95} = 0.35,$$

and the toroidal magnetic field on the plasma geometrical axis, and the total current in inductive mode of operation are taken to be:

$$B_{t_0} = 5.3 \text{ T}, \quad I_p = 15.0 \text{ MA}.$$

Using the plasma geometry description introduced in Chapter 2, we obtain the shape parameters of Table 4.1 measured from the ITER-FEAT elevation view. The comparison of the ITER-FEAT poloidal section with our modelling is shown in Fig. 2.9.

Table 4.1: Elongation, triangularity, and angles of the plasma X-points, for the upper and lower part of the last closed magnetic surface.

	upper part (1)	lower part (2)
κ_X	1.687	2.001
δ_X	0.466	0.568
Ψ^-	0	67.92°
Ψ^+	0	22.46°

The above data result in the following poloidal surface S_p, plasma volume V and surface S, aspect ratio A, effective elongation κ_a, and the safety factor of the cross section of the 95% magnetic flux surface $q_{\psi 95}$ calculated in the frame of our model:

$$S_p \simeq 21.8 \text{ m}^2, \quad V \simeq 827 \text{ m}^3, \quad S \simeq 684 \text{ m}^2,$$
$$A = 3.1, \quad \kappa_a \simeq 1.74, \quad q_{\psi 95} \simeq 3.03.$$

These values of plasma volume and surfaces are very close to those reported in Ref. [ODR99]: $S_p \simeq 21.9$ m^2, $V \simeq 837$ m^3, and $S \simeq 678$ m^2 (differences lower than 1.2% from the results of our model).

4.4 Profiles and impurities

The profiles are supposed to be of the generalized parabolic form (Eq. (3.25)). The density peaking profile is taken to be $\alpha_n = 0.01$, while the temperature peaking parameter α_T is calculated to reproduce the correct fusion power ($P_{\text{fus}} = 410$ MW) at the nominal operating point of ITER-FEAT [ODR99], i.e. $\langle T_i \rangle = 8.1$ keV, $\langle n_e \rangle = 1.014 \times 10^{20}$ m^{-3}, and $f_{\text{He}} = 4.1\%$. We obtain

$$\alpha_T \simeq 1.05.$$

The above value of α_T is a modelling of both the relatively peaked temperature profiles shown in Fig. 4.2, which would be represented[1] by $\alpha_T \simeq 2.2$, and the flattening due to saw-teeth.

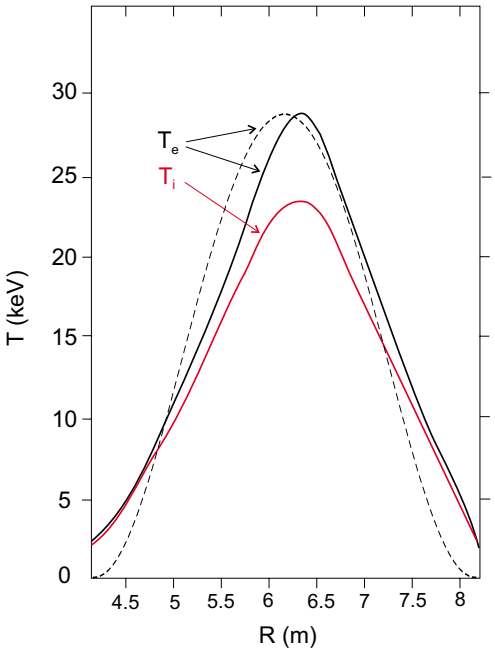

Figure 4.2: Temperature profiles of ITER-FEAT determined by the 1D code PRETOR for ions and electrons in red and black solid lines, respectively (source: Ref. [ODR99]). The best fitting generalized profile for the electron temperature (dashed line) corresponds to $\alpha_T = 2.2$.

The impurity fractions f_i are supposed to be constant for the two impurity species considered in this study: Beryllium and Argon, with

$$f_{\text{Be}} = 2\%, \quad f_{\text{Ar}} = 0.12\%.$$

[1] By the best fitting generalized parabolic profile.

The helium fraction f_{He} is calculated self-consistently imposing the ratio of the apparent helium confinement time to the energy confinement time $\tau^*_{\mathrm{He}}/\tau_E = 5$ [ASD98].

4.5 Other assumptions

- The synchrotron losses P_{syn} are calculated using the new fit derived in Section 3, with a reflection coefficient on the walls $r = 0.7$.
- The electron temperature is assumed to be approximately 10% higher than the ion temperature (according to Ref. [ODR99]):

$$\frac{T_e}{T_i} = \frac{8.9}{8.1} \simeq 1.10.$$

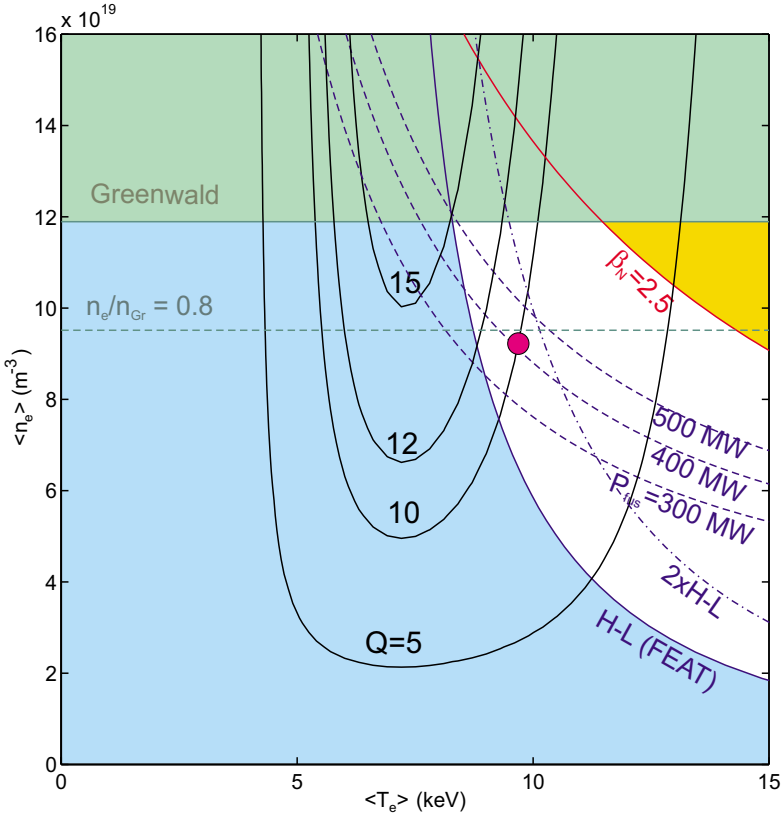

Figure 4.3: Q and P_{fus} contours for ITER-FEAT in inductive mode of operation, with H-mode regime and $\tau^*_{\mathrm{He}}/\tau_E = 5$, $\alpha_n = 0.01$, $\alpha_T = 1.05$, $f_{\mathrm{Be}} = 2\%$, $f_{\mathrm{Ar}} = 0.12\%$.

4.6 Inductive mode of operation

The reference confinement regime in the inductive mode of operation is a pure ELMy H-mode. For this analysis we consider the IPB98(y,2) scaling for the energy confinement time $\tau_E = H_{\rm H} \times \tau_{E,\rm IPB98(y,2)}$, with $H_{\rm H} = 1$.

In Fig. 4.3, for a couple of values of volume average temperature $\langle T_e \rangle$ and density $\langle n_e \rangle$ (denoted as operating point), the thermal equilibrium Eq. (2.1) is solved self-consistently for a ratio $\tau^*_{\rm He}/\tau_E = 5$ and for the other rules specified above, obtaining the corresponding additional heating power $P_{\rm add}$ (and amplification factor Q) and helium fraction $f_{\rm He}$. Then, for this operating point, we calculate the fusion power $P_{\rm fus}$, normalized beta $\beta_{\rm N}$, Greenwald density fraction $n/n_{\rm Gr}$, and margin to the H-L transition power $P_{\rm sep}/P_{\rm L\text{-}H}$. The curves plotted in Fig. 4.3 are the Q, $P_{\rm fus}$, $\beta_{\rm N}$, $n/n_{\rm Gr}$, and $P_{\rm sep}/P_{\rm L\text{-}H}$ contours. We see that the operating space with good confinement is the white area, which is limited by the MHD stability limits of density and beta ($n_e/n_{\rm Gr} \leq 1$ and $\beta_{\rm N} \leq 2.5$, respectively), and by the H-L transition.

The nominal operating point of ITER-FEAT at $Q = 10$ and $P_{\rm fus} = 410$ MW is reproduced. This point corresponds to an alpha heating power which is approximately double the additional heating power. Table 4.2 summarizes the main parameters for this point.

Table 4.2: Thermal balance for the nominal operating point in inductive mode of operation.

$\langle T_e \rangle$ (keV)	9.68	$P_{\rm fus}$ (MW)	410
$\langle n_e \rangle$ (10^{20} m^{-3})	0.92	P_α (MW)	83.0
Q	10	$P_{\rm OH}$ (MW)	0.89
τ_E (s)	3.19	$P_{\rm add}$ (MW)	40.1
$f_{\rm He}$ (%)	3.06	$P_{\rm source}$ (MW)	124
$Z_{\rm eff}$	1.67	$P_{\rm B}$ (MW)	18.3
$n_e/n_{\rm Gr}$	0.77	$P_{\rm syn}$ (MW)	5.32
$\beta_{\rm N}$	1.63	$P_{\rm rad\text{-}core}$ (MW)	23.6
$W_{\rm th}$ (MJ)	321	$P_{\rm con}$ (MW)	100
$\Phi_{\rm div\text{-}peak}$ (MW/m^2)	7.37	$P_{\rm rad\text{-}mantle}$ (MW)	26.8
$P_{\rm sep}/P_{\rm L\text{-}H}$	1.59	$P_{\rm sep}$ (MW)	73.7

It is interesting to note that this operating point at $q_{\psi 95} \sim 3$ meets the stability requirements of density ($n_e/n_{\rm Gr} \simeq 0.77$) and pressure ($\beta_N \simeq 1.63$). Moreover, assuming the H-L transition occurs when the separatrix power $P_{\rm sep}$ exceeds a threshold value $P_{\rm L\text{-}H}$, the H-mode regime is assured by approximately 60% of extra power crossing the separatrix. It is also seen that, assuming the simple formula (2.13) for the calculation of the peak heat flux on the divertor target plates $\Phi_{\rm div\text{-}peak}$, the consid-

ered radiative impurity content ($f_{\mathrm{Ar}} = 0.12\%$) is enough to assure a $\Phi_{\text{div-peak}}$ lower than the design value (10 MW/m^2).

The corresponding f_{He} contours are added in Fig. 4.4, giving $f_{\mathrm{He}} \simeq 3.06\%$ for the nominal operating point.

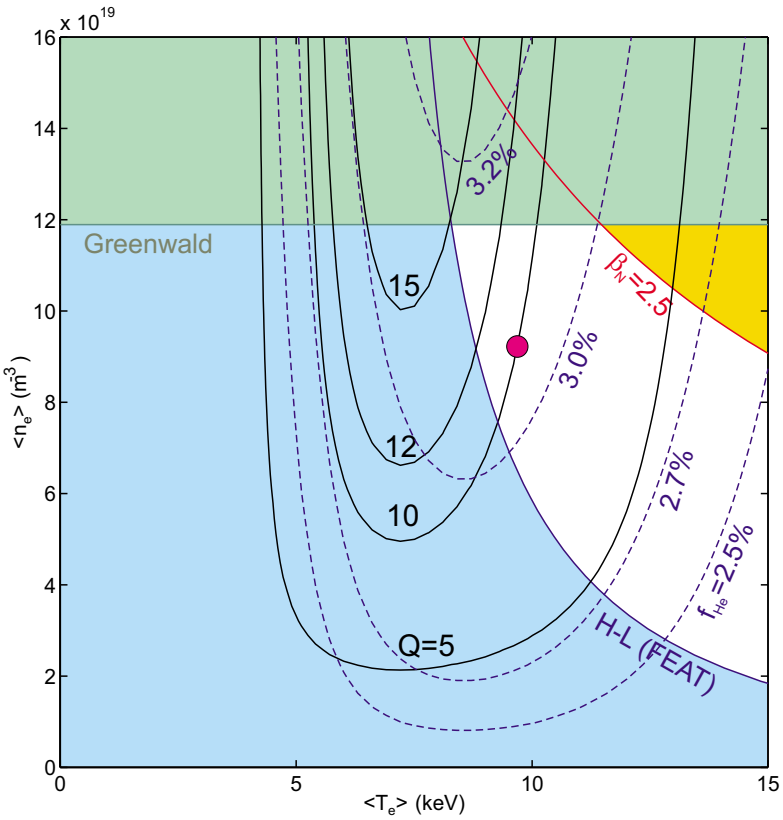

Figure 4.4: Q and f_{He} contours for ITER-FEAT in inductive mode of operation, with H-mode regime and $\tau^*_{\mathrm{He}}/\tau_E = 5$, $\alpha_n = 0.01$, $\alpha_T = 1.05$, $f_{\mathrm{Be}} = 2\%$, $f_{\mathrm{Ar}} = 0.12\%$.

4.6.1 Sensitivity of $\tau^*_{\mathrm{He}}/\tau_E$ to the plasma performance

The ITER-FEAT operating point displayed above assumes the ratio of the apparent helium confinement time to the energy confinement time to be equal to 5. Let us analyse the sensitivity of this parameter to the plasma projection performance in the inductive mode of operation.

For this study, the Greenwald density fraction and the H-L transition margin is kept constant with the nominal ITER-FEAT operating point obtained with our model (Table 4.2), i.e. $n_e/n_{\mathrm{Gr}} = 0.77$ and $P_{\mathrm{sep}}/P_{\mathrm{L\text{-}H}} = 1.59$. Next, we demonstrate

that using our plasma model and for a given device, the normalized beta pressure is fixed when the density and the H-L transition margin are constant. Indeed, for a given density n_e and according to Eqs (2.22) and (2.8), we have $P_{\text{net}}(n_e)$ and $\tau_E(n_e)$ which do not depend on temperature. Hence, by means of Eq. (2.9) it can be seen that the energy content W_{th} is also kept constant, and

$$C_W \int_V n_e T_e dV = \text{constant},$$

where the temperature T_e and the multispecies coefficient $C_W(f_{\text{He}})$ are variables. As the beta pressure is also proportional to $C_W \int_V n_e T_e dV$, we conclude that the normalized beta pressure is kept constant in the plasma equilibrium when varying $\tau^*_{\text{He}}/\tau_E$ (in the case of the ITER-FEAT operating point, we obtain $\beta_{\text{N}} \simeq 1.63$).

For each $\tau^*_{\text{He}}/\tau_E$ value we obtain the equilibrium point by solving self-consistently the power balance equation (Eq. 2.1). Fig. 4.5 shows the resulting evolution of Q and f_{He} versus the values of $\tau^*_{\text{He}}/\tau_E$ in the interval $[2, 10]$.

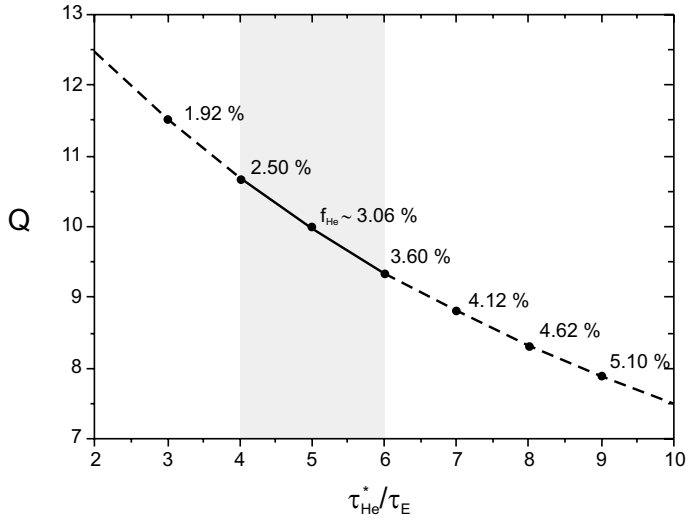

Figure 4.5: Amplification factor versus $\tau^*_{\text{He}}/\tau_E$ for points at thermal equilibrium, when keeping the density and the margin for the H-L power threshold equal to those obtained with our model in the inductive operating point ($n_e/n_{\text{Gr}} = 0.77$ and $P_{\text{sep}}/P_{\text{L-H}} = 1.59$). .

For plasmas with an ITER-like divertor, the ratio of apparent helium confinement time to the energy confinement time is supposed to be in the range of 4 to 6 [ASD98], which is the dotted area in Fig. 4.5. For this interval range, we observe that the plasma performance Q is weakly sensitive (less than 10%) to $\tau^*_{\text{He}}/\tau_E$.

4.6.2 Relationship between Q and the additional power P_{add}

The additional power P_{add} must fulfil the following main roles in ITER-FEAT operating scenarios:

1. provide a sufficient and continuous plasma heating power to access H-mode energy confinement in DT plasmas and subsequently to increase plasma temperatures to values where finite-Q driven burn ($Q = 10$) will occur,
2. providing a plasma start-up capability,
3. allow local control of the plasma current profile for plasma performance optimisation (advanced regimes) by controlling MHD activities,
4. providing a current drive capability to allow a non-inductive mode of operation (see Section 4.7).

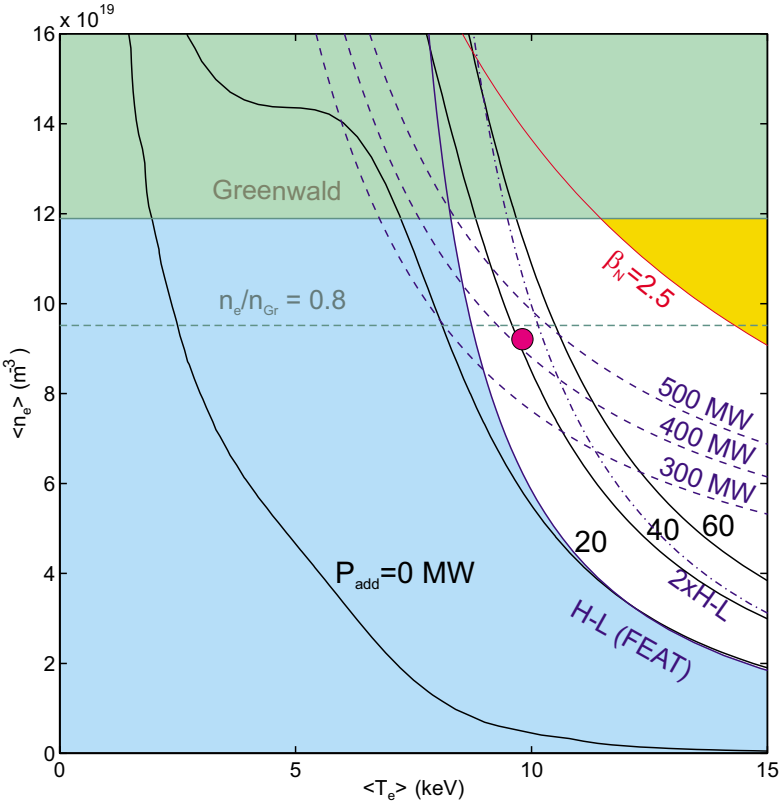

Figure 4.6: P_{add} and P_{fus} contours for ITER-FEAT in inductive mode of operation, with H-mode regime and $\tau^*_{\text{He}}/\tau_E = 5$, $\alpha_n = 0.01$, $\alpha_T = 1.05$, $f_{\text{Be}} = 2\%$, $f_{\text{Ar}} = 0.12\%$.

A combination of auxiliary systems is needed to provide flexibility and to extend the heating capability to a broad range of plasma parameters, e.g. $n_e = 0.3 - 1.3 \times 10^{20}$ m^{-3} and $T = 3 - 40$ keV. Neutral Beam Injection (NBI), ion cyclotron radio frequency (ICRF), electron cyclotron radio frequency (ECRF), and lower hybrid radio frequency (LHRF) wave heating systems are under consideration, and the ITER-FEAT device has been designed to accommodate up to 50 MW of any of these options.

The P_{add} contours in the plasma thermal equilibrium are plotted in the plane ($\langle T_e \rangle$,$\langle n_e \rangle$) (see Fig. 4.6), and the plasma performance Q versus the additional heating power is plotted in Fig. 4.7 for different contour curves (P_{fus}, n_e/n_{Gr}, $P_{\text{sep}}/P_{\text{L-H}}$, and β_{N}). In these diagrams it is shown that the first role of P_{add} is fulfilled for the ITER-FEAT parameters considered [ODR99]. On the one hand, the plasma temperature is increased enough to reach $Q = 10$ in inductive mode of operation, with a good margin with respect to stability constraints and objectives. On the other hand, H-mode is accessed with a power higher than 20-30 MW, as shown in Fig. 4.7 (the additional power required for the operating point is approximately 40 MW).

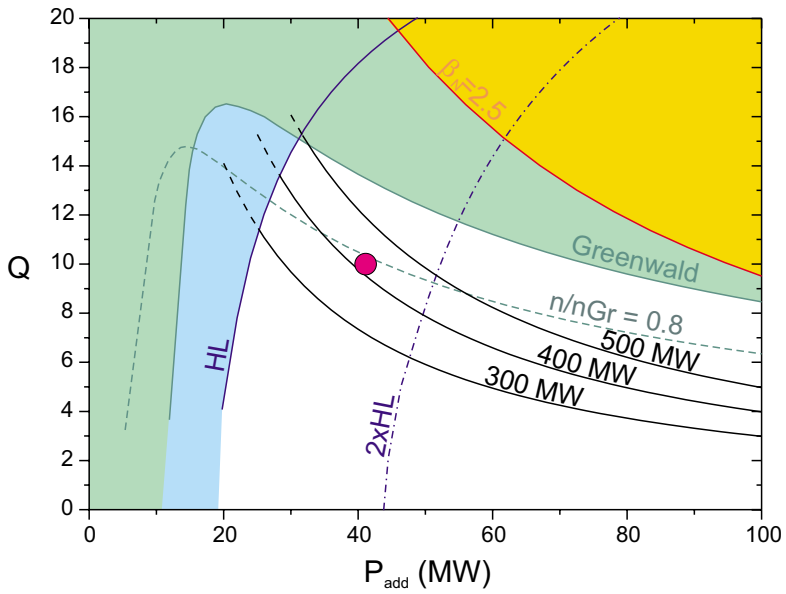

Figure 4.7: Plasma gain Q versus the addition heating power for the inductive mode of operation of ITER-FEAT.

4.6.3 Operating point with a softly mixed scaling

Owing to the fact that some concern has been expressed about a feasible degradation of the H-mode confinement below twice the value of the H-L power threshold [Jac98], a softly mixed scaling for the energy confinement time in inductive mode is next considered, in which the pure H-mode regime is accessed for $P_{\text{sep}}/P_{\text{L-H}} \geq 2$ (see Section 2.4.4). For $P_{\text{sep}}/P_{\text{L-H}} \leq 1$ the plasma confinement regime is the L-mode, whilst the middle case ($1 < P_{\text{sep}}/P_{\text{L-H}} < 2$) corresponds to a mixed L-H mode regime. The L-H transition function is defined in Eq. 2.23.

Fig. 4.8 shows the Q, β_{N}, n_e/n_{Gr} , and $P_{\text{sep}}/P_{\text{L-H}}$ contours for $\tau^*_{\text{He}}/\tau_E = 5$ using this softly mixed scaling for the energy confinement time. Note that Q contours are identical to those of a pure H-mode scaling (Fig. 4.3) for the region $P_{\text{sep}}/P_{\text{L-H}} \geq 2$. On the contrary, Q contours deviate from the H-mode behaviour for $P_{\text{sep}}/P_{\text{L-H}} < 2$. It can be seen that the point at minimum density for a given Q is situated close to the curve of twice the L-H transition power threshold ($P_{\text{L-H}}$), i.e. on H-mode or almost H-mode confinement regime. In other words, the optimum performance in inductive mode of operation considering the softly mixed L-H regime occurs at the H-mode (or almost H-mode) confinement regime.

Table 4.3: Thermal balance for the operating point in inductive mode of operation using a softly mixed τ_E scaling.

$\langle T_e \rangle$ (keV)	9.49	P_{fus} (MW)	492
$\langle n_e \rangle$ (10^{20} m^{-3})	1.02	P_{α} (MW)	99.7
Q	10	P_{OH} (MW)	0.87
τ_E (s)	2.90	P_{add} (MW)	48.4
f_{He} (%)	2.99	P_{source} (MW)	149
Z_{eff}	1.67	P_{B} (MW)	22.5
n_e/n_{Gr}	0.86	P_{syn} (MW)	5.34
β_{N}	1.79	$P_{\text{rad-core}}$ (MW)	27.8
W_{th} (MW)	351	P_{con} (MW)	121.1
$\Phi_{\text{div-peak}}$ (MW/m^2)	8.80	$P_{\text{rad-mantle}}$ (MW)	33.1
$P_{\text{sep}}/P_{\text{L-H}}$	1.79	P_{sep} (MW)	88.0

Although this mixed scaling for the energy confinement time is more restrictive than the pure H-mode one, a section of the $Q = 10$ curve appears to be in the region meeting the MHD stability limits of density and pressure ($n_e/n_{\text{Gr}} < 1$ and $\beta_N < 2.5$, respectively), which is the white area in the ($\langle T_e \rangle$,$\langle n_e \rangle$) plane of Fig. 4.8. The corresponding fusion power, however, is higher than 410 MW. The operating point of ITER-FEAT at $Q = 10$ and minimum P_{add} (plotted in Fig. 4.8), which corresponds approximately to the minimum density point of the Q curve, is detailed

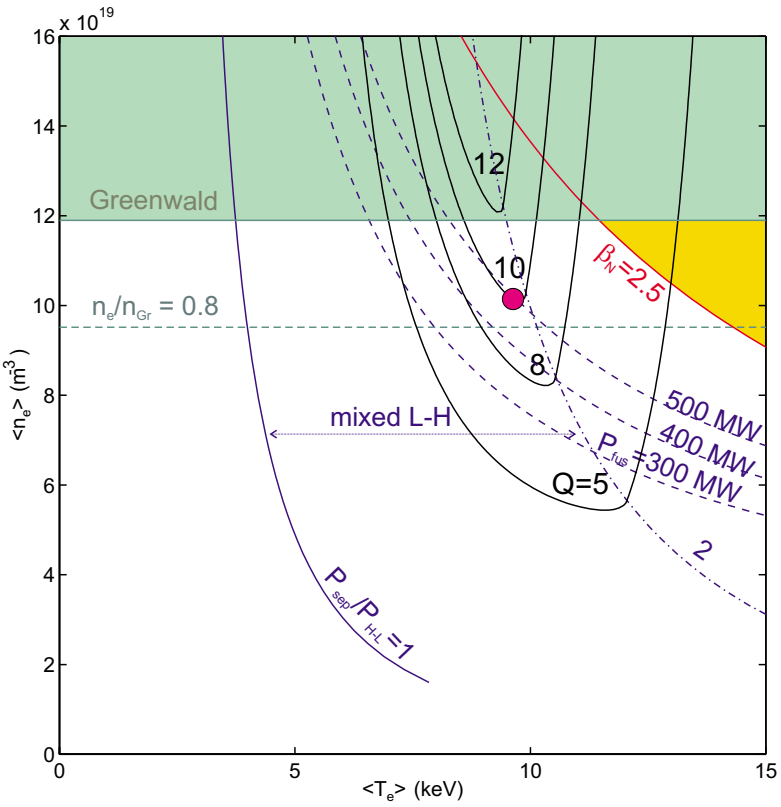

Figure 4.8: Q and P_{fus} contours for ITER-FEAT in inductive mode of operation, using a softly mixed scaling for τ_E and $\tau^*_{\text{He}}/\tau_E = 5$, $\alpha_n = 0.01$, $\alpha_T = 1.05$, $f_{\text{Be}} = 2\%$, $f_{\text{Ar}} = 0.12\%$.

in Table 4.3.

For this point, the parameter H^*_τ of Eq. (2.23) is approximately equal to 0.98. This means that the energy confinement time is obtained with 2% contribution from the L-mode scaling and with 98% contribution from the H-mode scaling. The required additional power ($P_{\text{add}} \simeq 48.4$ MW) remains compatible with ITER-FEAT design, and the margins to the MHD stability limits, especially the Greenwald density limit, have been reduced with respect to the nominal operating point in a pure H-mode regime, where the H-mode confinement is maintained until the power crossing the separatrix is equal to the L-H transition power threshold.

According to Eqs (2.8), (2.21), and (2.22), the power crossing the separatrix P_{sep} is higher than that of the nominal operating point in a pure H-mode regime due to a higher total plasma power and a similar density. As a result, the peak heat flux on the divertor target plates is also higher (8.8 MW/m^2 instead of 7.4 MW/m^2).

4.7 Steady-state operation

The capability of the ITER-FEAT designs for steady-state operation are studied numerically within the limitations of current assumptions and using the same plasma geometry, magnetic field, and impurities ($\tau^*_{\mathrm{He}}/\tau_E = 5$).

For this non-inductive mode of operation ($P_{\mathrm{OH}} = 0$), we assume the current drive efficiency to be proportional to the volume average temperature, in this way:

$$\gamma_{\mathrm{CD}} = \gamma_{0\mathrm{CD}} \langle T_e \rangle \qquad \text{with} \qquad \gamma_{0\mathrm{CD}} = 0.2 \times 10^{19} \ \mathrm{A\,m^{-2}/(W\,keV)}\,.$$

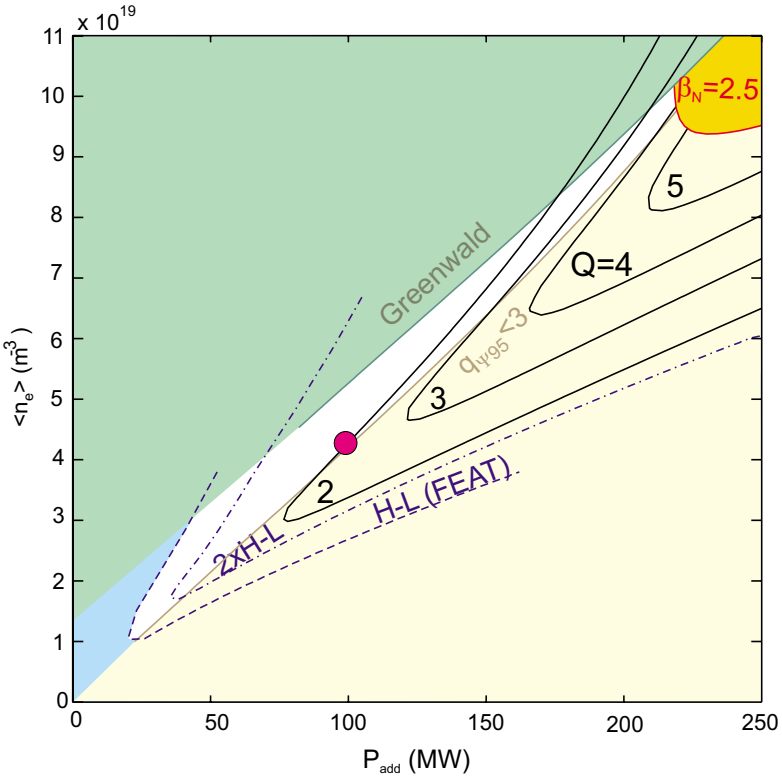

Figure 4.9: Q contours and density, pressure, and $q_{\Psi 95}$ stability limits in the plane $(P_{\mathrm{add}}, \langle n_e \rangle)$, for ITER-FEAT in steady-state operation with H-mode confinement regime and $\tau^*_{\mathrm{He}}/\tau_E = 5$, $\alpha_n = 0.01$, $\alpha_T = 1.05$, $f_{\mathrm{Be}} = 2\%$, $f_{\mathrm{Ar}} = 0.12\%$.

The role of the current drive efficiency on the plasma performance is discussed in Chapter 6.

4.7.1 H-mode conditions

Using the H-mode conditions ($H_{\rm H} = 1$, almost flat density profile $\alpha_n = 0.01$, and almost parabolic temperature profiles $\alpha = 1.05$), we obtain the current drive diagram shown in Fig. 4.9. The axis parameters are the additional power $P_{\rm add}$, which drives the non-bootstrap part $I_{\rm CD}$ of the plasma current, and the volume average density $\langle n_e \rangle$. Note that these are the two main control parameters for a continuous tokamak reactor.

As shown in the contour curves in inductive operation (see, as for example, Fig 4.3), the Q curves of the steady-state diagram are limited by the Greenwald density limit and by the beta pressure limit. Moreover, in non-inductive operation, the total current (and safety factor $q_{\Psi 95}$) is variable for each operating point in the diagram ($P_{\rm add}$, $\langle n_e \rangle$). Note that, as opposed to the inductive mode of operation, the highest plasma performance is not necessarily obtained at the maximum plasma current (due to the injected power dependence on the current drive, and to the bootstrap fraction enhancement for increasing values of $q_{\Psi 95}$). For the MHD stability of the plasma, we then impose the additional requirement $q_{\Psi 95} \geq 3$.

Fig. 4.9 shows the qualitatively narrow operational density interval. Assuming the current drive power capability available for ITER-FEAT to be $P_{\rm add} = 100$ MW [ODR99], as a combination of NBI and radio frequency power, the maximum plasma gain is reduced to $Q \simeq 2$.

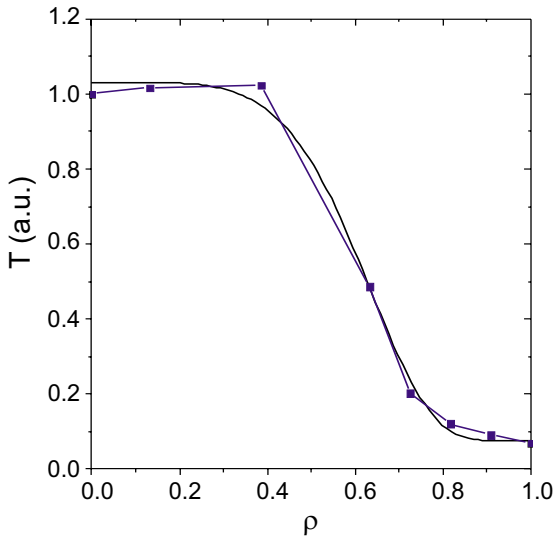

Figure 4.10: Comparison of the temperature profile of the optimized shear discharge #42940 (blue curve) with the best fit provided by Eq. (3.62) (black curve).

4.7.2 Advanced confinement regime

To reproduce the nominal operating point for ITER-FEAT in steady-state ($Q = 5$), we consider an advanced regime which enhances the energy confinement time with respect to the H-mode ($H_{\mathrm{H}} = 1.3$) and produces a strong density and temperature gradient. Thanks to this strong pressure gradient, the bootstrap current generation and consequently the total plasma current are improved. As a result, the plasma confinement is also improved.

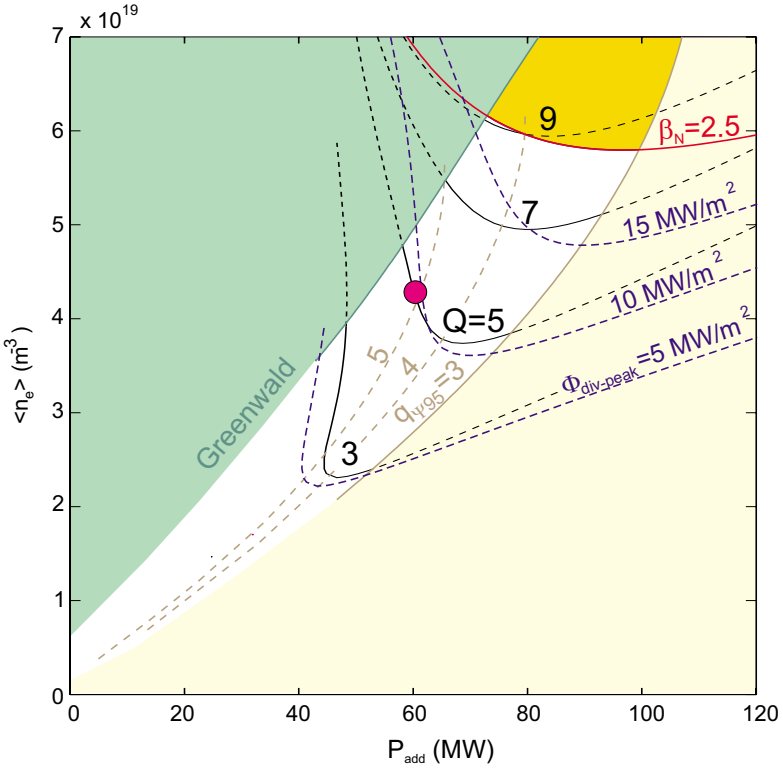

Figure 4.11: Q, $q_{\Psi 95}$, $\Phi_{\text{div-peak}}$ contours and stability limits in the plane (P_{add}, $\langle n_e \rangle$), for ITER-FEAT in steady-state operation with an advanced confinement regime and $\tau^*_{\text{He}}/\tau_E = 5$, $\alpha_n = 1.0$, $\alpha_T = 8$, $\beta_T = 5$, $f_{\text{Be}} = 2\%$, $f_{\text{Ar}} = 0.12\%$.

In such regimes, the temperature profile is not accurately described by a generalized parabolic profile (Eq. (3.25)) as the temperature is maintained to a high value up to a non-central layer. Fig. 4.10 shows the normalised temperature profile of an optimized shear discharge of JET (#42940) with internal transport barrier (ITB) compared with the best fitting parameters of the "advanced" radial dependence provided by Eq. (3.62) with $T_{e_a} = 1$ keV, giving

$$\alpha_T = 8 \quad \text{and} \quad \beta_T = 5.$$

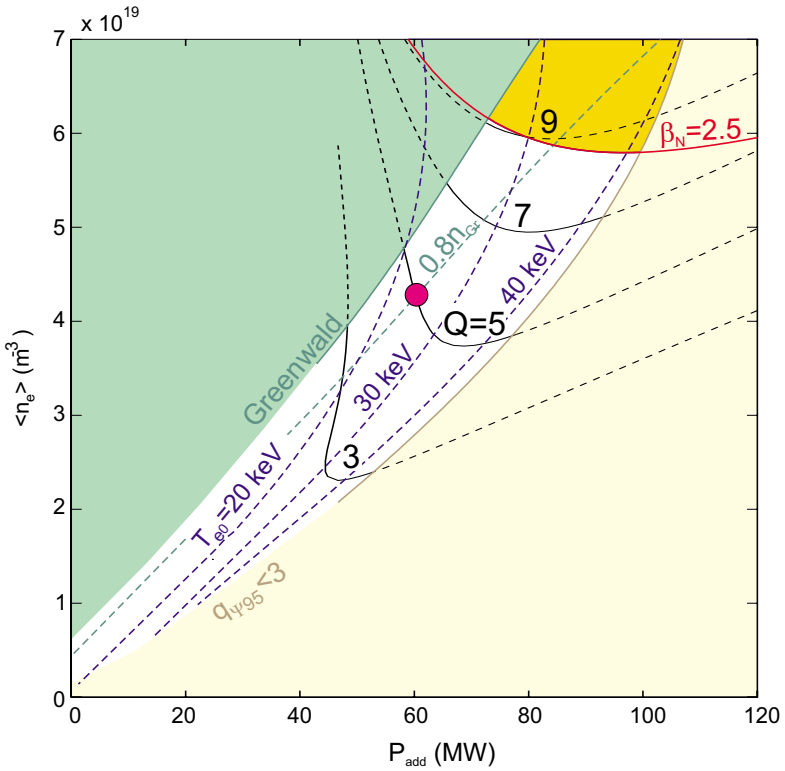

Figure 4.12: Q, T_{e_0} contours and stability limits in the plane (P_{add}, $\langle n_e \rangle$), for ITER-FEAT in steady-state operation with an advanced confinement regime and $\tau^*_{\text{He}}/\tau_E = 5$, $\alpha_n = 1.0$, $\alpha_T = 8$, $\beta_T = 5$, $f_{\text{Be}} = 2\%$, $f_{\text{Ar}} = 0.12\%$.

The current drive diagram for this advanced regime shows the Q contours as well as the curves of $q_{\Psi 95}$ and peak heat flux on the divertor target plates $\Phi_{\text{div-peak}}$ in Fig. 4.11, the central electron temperature T_{e_0} curves in Fig. 4.12, and the curves of bootstrap current fraction and helium fraction in Fig. 4.13.

In these conditions, the most restrictive constraint for working at high Q values is not the beta or $q_{\Psi 95}$ limits, or the maximum additional heating power installed. On the contrary, it is the peak heat flux on the divertor target plates $\Phi_{\text{div-peak}}$ which limits the performance. Considering a simple law for the $\Phi_{\text{div-peak}}$ calculation (Eq. 2.13), the $Q = 5$ objective in steady-state at 80% of the Greenwald density is achieved for $\Phi_{\text{div-peak}} \simeq 9.7$ MW/m^2, which is close to the nominal value for ITER-FEAT design (10 MW/m^2). This point corresponds to approximately $q_{\Psi 95} \simeq 5$, and to a bootstrap current fraction higher than 50%.

We obtain $Q \simeq 5.16$ at the point intersecting the curves $\Phi_{\text{div-peak}} = 10$ MW/m^2 and $n_e/n_{\text{Gr}} = 0.8$. Note also that $Q \sim 9$ could be obtained in the $\beta_{\text{N}} = 2.5$ limit if the peak heat flux on the divertor is pushed up to 20 MW/m^2.

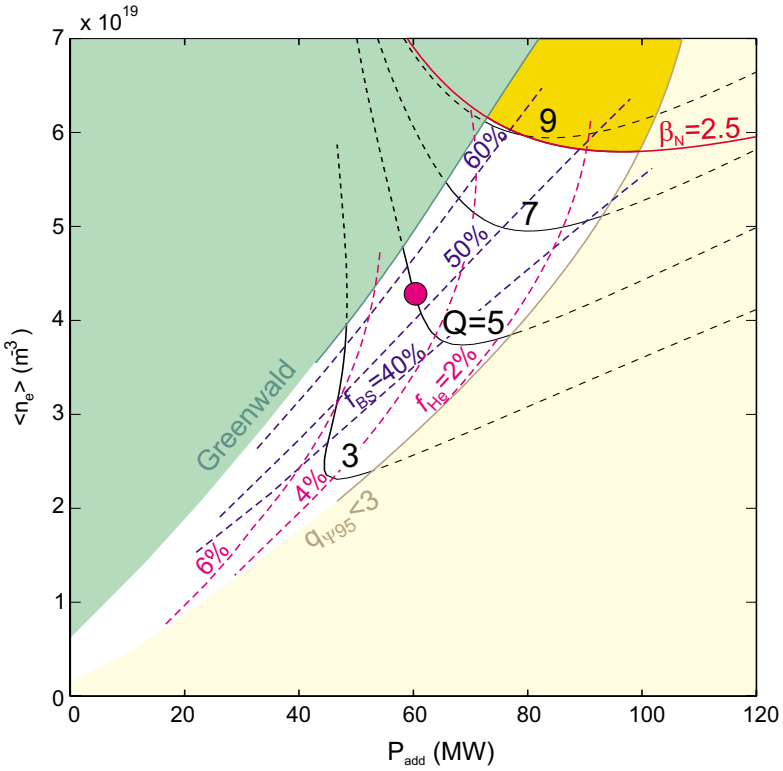

Figure 4.13: Q, f_{BS}, f_{He} contours and stability limits in the plane $(P_{\mathrm{add}}, \langle n_e \rangle)$, for ITER-FEAT in steady-state operation with an advanced confinement regime and $\tau^*_{\mathrm{He}}/\tau_E = 5$, $\alpha_n = 1.0$, $\alpha_T = 8$, $\beta_T = 5$, $f_{\mathrm{Be}} = 2\%$, $f_{\mathrm{Ar}} = 0.12\%$.

4.7.3 The role of density profile

To quantitatively evaluate the role of the peaking density profile on the performance of the current drive operating point, see in Fig. 4.14 the diagram obtained using an almost flat density profile, as the one characterizing the H-mode regime ($\alpha_n = 0.01$).

In this case, the maximum plasma gain is reduced to $Q \simeq 2.7$ when $\Phi_{\text{div-peak}}$ is kept to its nominal value. The evolution of Q versus the α_n density peaking parameter when imposing the density to be 80% of the Greenwald density and $\Phi_{\text{div-peak}} = 10$ MW/m^2, is shown in Fig 4.15 . The bootstrap fraction increases significantly when the density profile becomes peaked (from 41.5% to 54.1% for $\alpha_n = 0$ or 1, respectively) as well as the plasma gain Q.

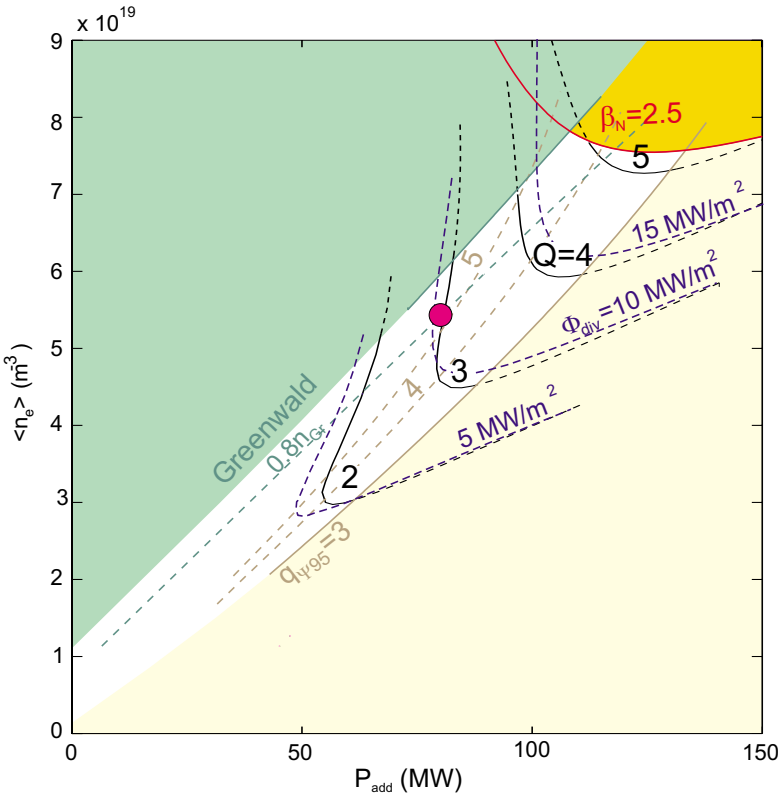

Figure 4.14: Q, $\Phi_{\text{div-peak}}$ contours and stability limits in the plane $(P_{\text{add}}, \langle n_e \rangle)$, for ITER-FEAT in steady-state operation with $H_{\text{H}} = 1.3$ and $\tau^*_{\text{He}}/\tau_E = 5$, $\alpha_n = 0.01$, $\alpha_T = 8$, $\beta_T = 5$, $f_{\text{Be}} = 2\%$, $f_{\text{Ar}} = 0.12\%$.

4.7.4 Optimal operating points in steady-state operation at $\Phi_{\text{div-peak}} = 10$ MW/m^2

Table 4.4 sums up the optimal operating points in steady-state operation when imposing the peak flux on the divertor target plates to its nominal value ($\Phi_{\text{div-peak}} = 10$ MW/m^2) and the density to 80% of the Greenwald limit ($n_e/n_{\text{Gr}} = 0.8$) for the advanced regime and for two density profiles (flat and peaked). For the H-mode regime, the optimal point at $\Phi_{\text{div-peak}} = 10$ MW/m^2 corresponds to the $q_{\Psi 95} = 3$ limit ($n_e/n_{\text{Gr}} \simeq 0.3$), as seen in Fig. 4.9. Here we use the ITER-FEAT plasma geometry, magnetic field, and impurities. The ratio of the apparent helium confinement time to the energy confinement time is imposed to $\tau^*_{\text{He}}/\tau_E = 5$, and an "advanced" temperature profile is considered with $\alpha_T = 8$ and $\beta_T = 5$.

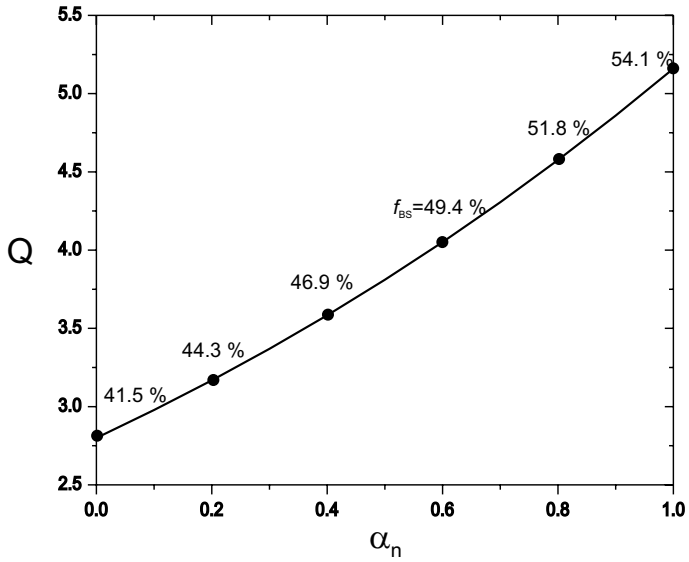

Figure 4.15: Q versus the peaking parameter for the density profile α_n at 80% of the Greenwald density and $\Phi_{\text{div-peak}} = 10$ MW/m^2, for ITER-FEAT in current drive mode of operation.

4.8 Summary

We conclude that, using the new model for the calculation of synchrotron losses (Chapter 3) as well as a detailed plasma geometry description, the $Q = 10$ and $Q = 5$ objective points of ITER-FEAT in inductive and current drive operation, respectively, are reproduced.

Sensitivity studies indicate that, in inductive operation, the ITER-FEAT device has good margins with respect to both the MHD stability limits. Assuming a purely H-mode regime when the separatrix power is higher than the L-H threshold power, approximately 40 MW of additional heating power enables access to the H-mode regime reaching $Q = 10$. On the other hand, when a softly mixed scaling for the energy confinement time is considered between $P_{\text{L-H}}$ and $2P_{\text{L-H}}$, the margins are slightly reduced and the additional power is increased to 48.4 MW, but the $Q = 10$ point is reached again in inductive mode of operation.

In non-inductive steady-state operation, we show that advanced tokamak regimes are required for achieving good thermonuclear plasma performance. In these regimes we assume a significant confinement improvement ($H_{\text{H}} \sim 1.3$) as well as a parabolic density profile, enhancing the bootstrap current generation. The performance analysis of such a mode of operation is carried out by means of the current drive diagram, which predicts self-consistently the plasma performance when imposing the addi-

Table 4.4: Optimal operating points in steady-state operation of an ITER-FEAT plasma with H-mode regime, with an advanced regime (AR) taking $H_{\mathrm{H}} = 1.3$, $\alpha_T = 8$, $\beta_T = 5$ and an almost flat density profile ($\alpha_n = 0.01$), and with an advanced regime (AR) taking $H_{\mathrm{H}} = 1.3$, $\alpha_T = 8$, $\beta_T = 5$ and a parabolic density profile ($\alpha_n = 1.0$).

	H-mode	AR($\alpha_n = 0.01$)	AR($\alpha_n = 1.0$)
$\Phi_{\text{div-peak}}$ (MW/m^2)	10	10	10
n_e/n_{Gr}	0.3	0.8	0.8
$q_{\Psi 95}$	3.0	5.46	5.04
I_{p} (MA)	15.6	8.34	9.03
T_{e_0} (keV)	30.6	27.2	24.1
n_{e_0} (10^{20} m^{-3})	0.37	0.53	0.86
$\langle T_e \rangle$ (keV)	17.4	10.2	9.09
$\langle n_e \rangle$ (10^{20} m^{-3})	0.37	0.53	0.43
f_{BS} (%)	14.6	41.7	54.1
Q	2.03	2.82	5.16
P_{add} (MW)	88.0	77.8	61.2
P_{fus} (MW)	179	219	316
P_{B} (MW)	3.96	5.16	7.32
P_{syn} (MW)	14.2	7.83	7.15
P_{con} (MW)	106	109	111
τ_E (s)	1.65	1.81	2.0
W_{th} (MJ)	234	198	221
f_{He} (%)	2.29	1.61	3.12
Z_{eff}	2.21	1.64	1.67
β_{N}	1.14	1.81	1.87

tional power and the plasma density. The most restrictive constraint for achieving higher Q values in steady-state operation is the peak heat flux on the divertor plates.